Eur. Phys. J. C (2022) 82:341
https://doi.org/10.1140/epjc/s10052-022-10309-w

THE EUROPEAN PHYSICAL JOURNAL C

Check for updates

Regular Article - Theoretical Physics

Ultraviolet properties of Lifshitz-type scalar field theories

Dario Zappalà[a]

INFN, Sezione di Catania, via S. Sofia 64, 95123 Catania, Italy

Received: 16 November 2021 / Accepted: 8 April 2022 / Published online: 20 April 2022
© The Author(s) 2022

Abstract We consider Lifshitz-type scalar field theories that exhibit anisotropic scaling laws near the ultraviolet fixed point, with explicit breaking of Lorentz symmetry. It is shown that, when all momentum dependent vertex operators are discarded, actions with anisotropy parameter $z = 3$ in 3+1 dimensions generate Lorentz symmetry violating quantum corrections that are suppressed by inverse powers of the momentum, so that the symmetry is sensibly restored in the infrared region. In the ultraviolet region, the singular behavior of the corrections is strongly smoothened: only logarithmic divergences show up, producing very small changes of the couplings over a range of momentum of many orders of magnitude. In the particular case where all couplings are equal, the theory shows a Liouville-like potential and quantum corrections are exactly summable, giving an asymptotically free theory. However, the observed weakening of the divergences is not sufficient to avoid a residual fine tuning of the mass parameter at a very high energy scale, in order to recover a physically acceptable mass in the infrared region.

1 Introduction

Understanding the ultraviolet (UV) structure of field theories is an essential issue to probe the mathematical consistency of the theory itself, but also to explore possible extensions or completions of models, such as the Standard Model of the elementary particle interactions and its interplay with General Relativity. Along this line, much effort has been devoted to find a way to smoothen the severe divergences that show up for instance in scalar theories, which are not protected by gauge symmetry. In particular, the inclusion of higher derivative operators has the effect of reducing the degree of UV divergence of the diagrams. This approach has the desired property of improving the renormalizability of the theory [1,2], and has been studied at length, both in the context of quantum field theories and in gravity [3–10].

In this regard, a helpful insight comes from condensed matter physics, where general properties of higher derivative theories have been related to the presence of Lifshitz points, i.e. points in the phase diagram at which it is observed the co-existence of a disordered phase, a spatially homogeneous ordered phase and a spatially modulated ordered phase, and their appearance is typically related to a particular balance between the standard two derivative term and a higher derivative term in the action [11–15]. Then, phase transitions associated to Lifshitz points can be put in relation with continuum limit and renormalizability properties of the related higher derivative euclidean field theory.

In general, condensed matter systems admit the existence of isotropic and anisotropic Lifshitz points as well, i.e. points that maintain full rotational symmetry on all coordinates, the former, and points that present anisotropic scaling properties and are described by two different correlation lengths in different space directions, the latter. Accordingly, isotropic points require a symmetric structure of the higher derivative terms that involves the same order of derivatives for each coordinate, while anisotropic points are characterized by different number of derivatives on different coordinates. Therefore, properties of the transitions and dependence on dimensionality are different in the two cases.

Although the isotropic case possesses a rich phase structure [11,15–20], only the anisotropic case can meaningfully be connected with field theories defined in Minkowski space, that are of interest in the high energy context. In fact, the presence of time derivatives of order larger than two directly leads to the Ostrogradski instability, corresponding to Hamiltonians unbounded from below with violation of unitarity [4,21]. To avoid these complications, it is unavoidable to resort to anisotropic Lifshitz systems where the time derivative is of second order, while in the spatial sector higher derivative terms are present (usually the anisotropy parameter z is intro-

[a] e-mail: dario.zappala@ct.infn.it (corresponding author)

duced to specify the order of the spatial derivatives as equal to $2z$).

Even in anisotropic form, the Lifshitz points have the effect of enhancing the UV sector of the theory, reducing the degree of divergence. The price to pay is the breaking of Lorentz invariance at high energy scales, and it becomes essential to verify that Lorentz symmetry becomes manifest in the infrared (IR) region [22], due to a suppression of the Lorentz breaking terms below the level of the experimental limits.

This kind of anisotropic models received much attention, especially after the introduction of the Hořava–Lifshitz formulation of the gravitational theory [23] with the aim of deriving a renormalizable approach to quantum gravity, and a lot of work has followed in various contexts ranging from gravity, black holes, cosmology [24–35], to gauge, scalar or fermionic field theory [36–43]. In particular, in [37] and subsequently in [41] it was pointed out that anisotropic scalar theories which include all possible renormalizable operators (according to the Lifshitz scaling), have the serious drawback of producing large Lorentz violating quantum corrections that are not compatible with the experimental observations, unless a quite severe fine tuning of various couplings in the UV region is performed.

In this paper, we reconsider this problem and select a specific class of scalar theories that avoids the occurrence of the large Lorentz violating corrections. We shall focus on a $3+1$-dimensional theory with anisotropy parameter $z=3$, because of its particular Lifshitz point structure and then, after reducing the bare action to momentum independent vertices only, we analyze the generated quantum corrections. Since Lorentz symmetry is absent from the beginning, we are allowed to treat divergent terms by means of a non-Lorentz invariant regulator, namely a three-momentum cut-off and, due to the very simple nature of the divergent diagrams, we are able to carry out our computations without resorting to the rotation to Euclidean coordinates, in the spirit of [44,45]. Within this approach the main interesting properties of the renormalized theory are pointed out and the crossover from the UV to the IR region is analyzed.

In Sect. 2, we study the properties of Lifshitz scaling of higher derivative scalar field theories and their consequently modified renormalizability. In Sect. 3, we analyze one specific model with $z=3$ and its diagrammatic expansion, while in Sect. 4 the RG flow of the various couplings in the UV and IR regimes. The conclusions are reported in Sect. 5.

2 Lifshitz scaling

We are specifically interested in the following Minkowskian Action

$$S=\int d^3x\,dt\left(\frac{1}{2}\left(\partial_t\phi\right)^2-\frac{\widehat{a}_z}{2}\left(\partial_i^z\phi\right)^2-\frac{\widehat{a}_{z-1}}{2}\left(\partial_i^{z-1}\phi\right)^2 -\cdots-\frac{\widehat{a}_1}{2}\left(\partial_i\phi\right)^2-V\right), \tag{1}$$

where we included higher derivatives of the spatial coordinates labelled by the index i (and i is summed over $i=1,2,3$), up to order $2z$ (with $z>1$). Hatted couplings indicate that they are dimensionful quantities. This is a particular case of the general problem of anisotropic Lifshitz scaling where the full set of Euclidean coordinates is composed of two subsets which have different scaling properties in proximity of a Lifshitz point. In the case of Eq. (1), one subset is represented by the time coordinate and the other by the 3 spatial coordinates, with scaling dimensions respectively $[t]_s=-z$ and $[x^i]_s=-1$, so that for a scale transformation with rescaling parameter $b>1$, one observes the following non-uniform scaling of space and time

$$t\to b^z\,t,\qquad x^i\to b\,x^i. \tag{2}$$

This leads to a substantial difference with respect to the standard scaling associated with the canonical dimensions of the parameters entering Eq. (1) which occurs in proximity of the gaussian fixed point.

So, for instance, the coefficients $\widehat{a}_j$ (with $j>1$) of the higher derivative terms appearing in Eq. (1), have negative canonical dimension and, accordingly, the corresponding terms are perturbatively non-renormalizable. However the presence of another fixed point, the Lifshitz point, ensures different scaling rules that redefine the renormalization properties of the various terms and, in accordance with the scaling rules in Eq. (2), we derive the scaling dimension of the field from the scaling properties of the term proportional to $\widehat{a}_z$ (which is assumed to have scaling dimension $[\widehat{a}_z]_s=0$) :

$$[\phi]_s=\frac{3-z}{2}\,. \tag{3}$$

Actually, this is a particular case of a more general analysis of a d-dimensional system with d_s dimensions in one subset of coordinates, instead of the 3 spatial dimensions, and $d-d_s$ dimensions in the other subset, instead of the only time dimension. In fact, in general by allowing for an anomalous dimension η of the d_s-dimensional subset, i.e. by redefining the scaling dimension $[\widehat{a}_z]_s=-\eta$, one obtains $[\phi]_s=[z\,(d-d_s-2)+d_s+\eta]/2$, that clearly reproduces Eq. (3) for $d=3+1$, $d_s=3$ and $\eta=0$. Nevertheless, for our purposes of analyzing a (3+1)-dimensional Minkowskian space-time theory, it is sufficient to retain the scaling rule in Eq. (3) with zero anomalous dimension.

Once the scaling dimension of the field is known, we can investigate the constraints on the various parameters that characterize the existence of a non-trivial Lifshitz point and, in general, this means finding the upper and lower critical

dimension for the action considered. In our case, where the dimensions are kept fixed, this reduces to a constraint on z. In fact, by considering the potential in Eq. (1) as an expansion in powers of the field

$$V = \sum_{n=2}^{\overline{n}} \frac{\widehat{g}_n}{n!} \phi^n \quad , \tag{4}$$

we easily derive the scaling dimension of the generic $\widehat{g}_n$:

$$[\widehat{g}_n]_s = \left(1 - \frac{n}{2}\right)(z+3) + nz \tag{5}$$

and therefore, the marginality condition $[\widehat{g}_n]_s = 0$ corresponds to the constraint

$$(2+n)\, z = 3\,(n-2)\,. \tag{6}$$

From Eq. (6), we find that, when $z = 1$, the marginal coupling corresponds to $n = 4$, as is well known, and when $z = 2$ to $n = 10$, and when z=3 no finite n satisfies Eq. (6) as $[\widehat{g}_n]_s = 6$ for any n.

By inverting the argument, if we require the marginal coupling to be $\widehat{g}_4$ so that, at least for theories with Z_2 symmetry (or $O(N)$ symmetry for a multicomponent field), no term in the potential (4) has positive scaling dimension (apart from the quadratic mass term), we find that in Eq. (6), $[\widehat{g}_4]_s = 0$ implies $z = 1$. This indicates that our 3+1 dimensional system with $z = 1$ corresponds to the upper critical dimension which instead becomes larger at larger values of z. On the other hand, the lowest dimension below which the non-trivial Lifshitz point disappears, corresponds to the vanishing of the scaling dimension of the field. According to Eq. (3), for our 3+1 dimensional system this implies $z = 3$.

The above analysis indicates that for a $O(N)$ theory in 3+1 dimensions, a non-trivial Lifshitz point is expected for $z = 2$ only, while when $z = 1$ and $z = 3$ we are respectively at the upper and lower critical dimension of the system where only the trivial Lifshitz point solution of the Renormalization Group analysis is found. Namely, it corresponds to the quadratic action with, respectively, $z = 1$ and $z = 3$:

$$S_{FP} = \int d^3x\, dt \left(\frac{1}{2}\,(\partial_t \phi)^2 - \frac{\widehat{a}_z}{2}\left(\partial_i^z \phi\right)^2\right) . \tag{7}$$

These results are totally in agreement with those of [12,14,46] where the existence of a Lifshitz point solution is investigated for generic number of dimensions of the two subsets of coordinates and with $z = 2$ fixed. Clearly, if $z = 1$ in Eq. (7), we are left with the standard Gaussian fixed point, while $z = 3$ yields a non-standard higher derivative action that we expect to be responsible for a well behaved UV sector of the theory.

In fact, it is easy to realize that when $z = 3$, the scaling dimension of the field vanishes according to Eq. (3), and therefore all possible interaction terms (and mass term) that can be added to S_{FP} have couplings with positive scaling dimension, which means that these operators are relevant with respect to to this fixed point solution and get suppressed in the UV regime. This is in agreement with the naive expectation that the UV divergences of such a higher derivative theory with $z = 3$ are strongly (if not totally) suppressed by the enhanced power of the momentum (k^6 instead of k^2) in the propagator.

Therefore, since we want to investigate how much the fixed point solution (7) does protect from the UV divergences, we shall consider the most favourable case with $z = 3$. Moreover, for $z = 2$, the appearance of the non-trivial Lifshitz point in addition to the one of (7), does certainly modify the structure of Renormalization Group flow and this could generate some complication in the renormalization process. On the other hand, larger values of z, such as $z = 4$, imply a negative scaling dimension of the field, thus producing an unstable theory.

In conclusion we will focus on the action in Eq. (1) with $z = 3$ and the potential V specified in Eq. (4), with generic $\overline{n}$. In fact, as it will be shown next, the divergence of the loop diagrams of this theory does not depend on the index n that defines the number of legs of each vertex.

We turn now to the analysis of the degree of divergence of the various loop diagrams of such a theory and, since we are including in the action (1) an explicit violation of the Lorentz symmetry, we are allowed to treat space and time coordinates separately in the loop integrals. Then, we find convenient to maintain Minkowskian coordinates, thus avoiding the rotation to Euclidean coordinates, and to first perform the integration on the energy component in the four-momentum integral along the Feynman contour, so that the divergences appear only in the integration on the three momentum. We shall take care of them by means of a Lorentz violating three-momentum cut-off Λ.

In order to compute the degree of divergence of a generic diagram, we recall the well known fact that each propagator can be split into the product of two factors, with one of the two being a pole of the energy integral. So for instance, in a one loop integral with two propagators we end up with the product of four terms, two of which give poles that are relevant in the Feynman contour integration :

$$\begin{aligned} R_1(p) &= \int \frac{d^3k\, dk_0}{(2\pi)^4} \frac{1}{\left[k_0^2 - A^2 + i\epsilon\right]} \\ &\quad \frac{1}{\left[(p_0+k_0)^2 - B^2 + i\epsilon\right]} \\ &= \int \frac{d^3k\, dk_0}{(2\pi)^4} \frac{1}{[k_0 - A + i\epsilon]\,[k_0 + A - i\epsilon]} \\ &\quad \times \frac{1}{[(p_0+k_0) - B + i\epsilon]\,[(p_0+k_0) + B - i\epsilon]}\,, \end{aligned} \tag{8}$$

where we defined, according to the action (1) with $z = 3$ and the potential (4),

$$A = \sqrt{\widehat{a}_3\,\vec{k}^{\,6} + \widehat{a}_2\,\vec{k}^{\,4} + \widehat{a}_1\,\vec{k}^{\,2} + \widehat{g}_2} \quad ,$$
$$B = \sqrt{\widehat{a}_3\,(\vec{p}+\vec{k})^{\,6} + \widehat{a}_2\,(\vec{p}+\vec{k})^{\,4} + \widehat{a}_1(\vec{p}+\vec{k})^{\,2} + \widehat{g}_2}. \quad (9)$$

We then perform the integration over k_0 by reducing the double pole to a sum of simple poles, according to the expression:

$$\frac{1}{x-P_1}\;\frac{1}{x-P_2} = \left(\frac{1}{x-P_1} - \frac{1}{x-P_2}\right)\frac{1}{(P_1-P_2)}\;, \quad (10)$$

where x indicates the integration variable and P_1, P_2 are x-independent expressions.

The outlined procedure can be extended also to multi-loop diagrams and this allows us to infer the rule to count the degree of divergence of each diagram. In fact, after performing the integrations on the energy component of every loop, we find for generic z (which is then set to $z = 3$ in our model) that each loop brings 3 powers of momentum from the three-momentum integration, while each internal line contributes with $-2z$ powers of momentum, with the exception of one internal line for each loop that contributes with a power equal to $-z$, because of the cancellation produced by the integration over k_0. With the help of this rule we compute the degree of divergence of a diagram (i.e. the powers of the three-momentum cut-off Λ) D_Λ:

$$D_\Lambda = [3L - 2z\,(I-L) - z\,L]\,|_{z=3} \;=\; 6(L-I) \quad (11)$$

where L is the number of loops and I the number of internal lines of the diagram (below, we shall label the number of external lines as E and the number of vertices with n lines as V_n).

If we now recall the well known relations due to the diagram topology, $L = I - \sum_n V_n + 1$ and $\sum_n (n\,V_n) = E + 2I$, where the sum is understood over the kind of vertices entering the diagram, we obtain from Eq. (11) :

$$D_\Lambda = \left[\left(\sum_n (nV_n) - E\right)\frac{(3-z)}{2} + (3+z)\left(1 - \sum_n V_n\right)\right]\Bigg|_{z=3} = 6\left(1 - \sum_n V_n\right). \quad (12)$$

Incidentally, the same conclusions would have been obtained had we inspected the divergence structure of the theory after Wick rotation to Euclidean coordinates and adopted a symmetric cut-off on the modulus of the four-momentum in the loop integrals.

It is now evident that, in the presence of modified 'higher derivative' propagators with $z = 3$, only logarithmic divergences show up in diagrams containing only one vertex, whatever is the value of n and the number of external legs E. Consequently the UV sector of such a theory turns out to be rather simple and we shall analyze it in Sect. 3.

One could object that the action (1) with $z = 3$ does not include all renormalizable terms, because the scaling dimension of the field is vanishing, as shown in Eq. (3). Therefore, besides including any possible value of n, which characterizes the vertex in the potential (4), it is admissible to include also vertices like

$$w_{m,s}\;\phi^m\left(\partial_i^s\phi\,\partial_i^s\phi\right)\;, \quad (13)$$

with positive integer m and $s = 1, 2, 3$, still maintaining non-negative scaling dimension of the corresponding coupling (higher values of s would instead yield negative scaling dimension). Clearly, such kind of vertex that brings a dependence on the momentum of two lines, does increase the degree of the divergence when the momentum of these two lines involves the integrated internal momentum of a loop, and therefore it requires a more accurate rearrangement of all the diverging integrals in the renormalization procedure; but nevertheless the renormalizability property guarantees the full cancellation of divergences by suitable insertion of counterterms.

On the other hand, there is one important property concerning the class of vertices in Eq. (13) that must be considered. Namely, the requirement $w_{m,s} = 0$, for all $m > 0$ and $s = 1, 2, 3$ in the bare action (1) of our model, implies the absence of any UV divergence in the following expansion of the $(m+2)$-point Green functions generated by the action (1), with m out of the $(m+2)$ momenta set to zero:

$$(p_i\,p_i')^s\;\;\mathcal{W}_{m,s} = (p_i\,p_i')^s\left[\left(\frac{\partial^2}{\partial p_j\;\partial p_j'}\right)^s\Gamma^{(m+2)}(p,\,p',0,\ldots,0)\right]_{p=p'=0}. \quad (14)$$

The relevance of this property is clear. In fact any UV divergence in terms like $\mathcal{W}_{m,s}$ in Eq. (14) could not be cancelled, because this is achievable only by means of a counterterm generated by the corresponding vertex in (13) that, however, is missing in the bare action (1) where we set all $w_{m,s} = 0$.

To prove the above statement, we notice that, without vertices (13) in the bare action, the only way to get an explicit dependence on the external momenta to the power $2s$, analogous to the $2s$ derivatives in Eq. (13), is given by the expansion in Eq. (14). In addition, it is evident that the external momenta dependence of a Green function of the action (1), which is essential to obtain non-vanishing derivatives in Eq. (14), cannot be generated by diagrams with one vertex only, but comes instead from diagrams containing at least two vertices.

Then, with all $w_{m,s} = 0$ in (1), D_Λ must be read from Eqs. (11) and (12), and, as we had already observed, it implies that only diagrams with one vertex are UV divergent. Therefore, Green functions that carry external momentum dependence

and consequently contain at least two vertices, are finite. This is already sufficient to demonstrate our statement but, since $\mathcal{W}_{m,s}$ is the result of $2s$ derivatives with respect to the external momenta of such a Green function, we have a further increase of the degree of UV convergence of $\mathcal{W}_{m,s}$, as compared with $\Gamma^{(m+2)}(p, p', 0, \ldots, 0)$.

We conclude that the constraint $w_{m,s} = 0$ for all $m > 0$ and $s = 1, 2, 3$ is sufficient to warrant only UV finite contributions to $\mathcal{W}_{m,s}$, which are harmless in the analysis of the renormalized theory, in much the same way as the $g_4\,\phi^4$ vertex in the action of a standard renormalizable theory in four dimensions generates only UV finite $\Gamma^{(n)}$ Green functions with $n \geq 6$, while the inclusion of the $g_6\,\phi^6$ vertex, which produces unmanageable UV divergences, would instead spoil the UV convergence of those Green functions.

At this point, we recall that momentum dependent vertices in Eq. (13) are responsible of another undesired feature, as shown in [37]. In the latter, a 4+1 dimensional model with $z = 2$ is studied, but the effect produced by these momentum dependent vertices is essentially the same in their case and in ours. More specifically, if we compute the one loop correction to the coefficient a_1, generated by the term $\phi^2\,(\partial_i\phi\partial_i\phi)$, of the kind displayed in Eq. (13), suitably included into the action (1), we get logarithmic corrections to a_1. Then, if we compare the logarithmic corrections obtained for two different kind of fields with different couplings, we find that the renormalized a_1 of the two fields differ by a logarithmically growing quantity when the IR region is approached, unless a fine tuning of the couplings of the two fields in the UV region is enforced. This discrepancy, as discussed in [37], is certainly not compatible with the observed Lorentz invariance in the IR region, that requires instead equal renormalized a_1 for the two fields, at least within the experimental errors. (For a detailed review about IR effects of Lorentz invariance violation introduced at extremely large energy scales and, in particular, with reference to quantum gravity models, see [47,48]).

As these logarithmic corrections, unacceptable on phenomenological grounds, disappear if the momentum dependent vertices in Eq. (13) are omitted from the full action, leaving only finite power law corrections to the dispersion relation (as will be discussed in Sect. 3), we choose to bypass the renormalizability criterion that would instead require the inclusion of the terms displayed in Eq. (13). In other words, the action in (1) analyzed in Sect. 3, contains all renormalizable operators, according to the Lifshitz scaling around the fixed point solution (7), with the exception of momentum dependent vertices; the couplings associated to the latter will be set to zero in the bare action. The evidence that, under these assumptions, $\mathcal{W}_{m,s}$ in Eq. (14) gets only UV finite corrections, guarantees the consistency of our choice.

3 Renormalized theory

According to the issues considered in Sect. 2, we restrict our analysis to the action

$$S = \int d^3x\,dt\left[\frac{1}{2}\,(\partial_t\phi)^2 - \frac{\widehat{a}_3}{2}\left(\partial^2\partial_i\phi\partial^2\partial_i\phi\right) - \frac{\widehat{a}_2}{2} \times \left(\partial^2\phi\partial^2\phi\right) - \frac{\widehat{a}_1}{2}\,(\partial_i\phi\partial_i\phi) - V(\phi)\right], \tag{15}$$

with V given in Eq. (4) and where, in order to keep the number of couplings finite, we choose the maximum power of the field, $\overline{n}$, finite. Note that any other term, quadratic in the field and containing 2 or 4 or 6 derivatives but with different derivative ordering with respect to Eq. (15), like e.g. $\left(\partial_i\partial_j\partial_k\phi\;\partial_i\partial_j\partial_k\phi\right)$ or $\left(\partial_i\partial_j\phi\;\partial_i\partial_j\phi\right)$, is always reducible, after integration by parts, to one of the terms in (15).

It is now convenient to redefine the various hatted couplings in terms of adimensional couplings by means of the mass parameter M, which we take much larger than the typical energy scales that characterize the IR physics of this model. Therefore :

$$\widehat{a}_s = \left.\frac{a_s}{M^{2(s-1)}}\right|_{s=1,2,3}; \qquad \widehat{g}_n = \left.\frac{g_n}{M^{n-4}}\right|_{n=2,3,4,\ldots} \tag{16}$$

Moreover, in order to set the overall scale of the action, the coefficient of the time derivative of the field in Eq. (15) is taken equal to one , and, in addition, a relative rescaling of the space and time allows us to take $a_1 = 1$ and, finally, a redefinition of the mass scale M can be performed to set also $a_3 = 1$, while a_2 remains an unconstrained coupling. Thus, we take :

$$\widehat{a}_3 = \frac{a_3}{M^4} = \frac{1}{M^4}; \qquad \widehat{a}_1 = a_1 = 1\ . \tag{17}$$

Now we turn to the computation of the quantum corrections. In Sect. 2 we verified that the divergent diagrams generated by this model must contain at most one vertex, which means that we have only one logarithmically divergent integral, namely

$$\widehat{I}_1 = \int \frac{d^3k\;dk_0}{(2\pi)^4}\,\frac{i}{\left(k_0^2 - \widehat{a}_3\vec{k}^{\,6} - \widehat{a}_2\,\vec{k}^{\,4} - \widehat{a}_1\vec{k}^{\,2} - \widehat{g}_2 + i\epsilon\right)} = \frac{1}{2}\int \frac{d^3k}{(2\pi)^3}\,\frac{1}{\sqrt{\widehat{a}_3\vec{k}^{\,6} + \widehat{a}_2\,\vec{k}^{\,4} + \widehat{a}_1\vec{k}^{\,2} + \widehat{g}_2}} \tag{18}$$

In Eq. (18) we performed the integral in k_0 and we are left with the integral over the three-momentum $\vec{k}$ that will be calculated for $|\vec{k}|$ between the UV cut-off Λ and an IR cut-off which we choose, for the moment, equal to M in order to neglect, in first approximation, other smaller scales such as $\widehat{g}_2$:

$$\widehat{I}_1(\Lambda, M) = M^2\, I_1(\Lambda, M) = \frac{M^2}{(2\pi)^2}\, \ln\left(\frac{\Lambda}{M}\right) + O\left(\frac{M^4}{\Lambda^2}\right) \tag{19}$$

If we now focus on the quantum corrections for the quartic coupling $\widehat{g}_4 = g_4$, we notice that the collection of divergent, single vertex diagrams includes the sum of the diagram with vertex $\widehat{g}_6$ and the one loop integral $\widehat{I}_1$, plus the diagram with vertex $\widehat{g}_8$ and two loops corresponding to the square of the integral $\widehat{I}_1$, and so on, until the last diagram with $\widehat{g}_{\overline{n}}$ and $\widehat{I}_1^{(\overline{n}/2-2)}$. After counting the combinatorial factors and by making use of the adimensional couplings, we get the renormalized quartic coupling g_{4R}

$$g_{4R} = g_4 + g_6\left(\frac{I_1}{2}\right) + \frac{g_8}{2}\left(\frac{I_1}{2}\right)^2 + \frac{g_{10}}{3!}\left(\frac{I_1}{2}\right)^3 + \cdots + \frac{g_{\overline{n}}}{(\overline{n}/2-2)!}\left(\frac{I_1}{2}\right)^{(\overline{n}/2-2)} \tag{20}$$

where we assumed $\overline{n}$ to be an even integer (for odd $\overline{n}$, one has just to replace $\overline{n}$ with $(\overline{n}-1)$ in Eq. (20)).

Moreover, the structure of this series of diagram is such that when we compute g_{6R} or g_{8R}, we get exactly the same series as in Eq. (20), with the only difference that each coupling index is increased of 2 units (for g_{6R}) or 4 units (for g_{8R}), while the truncation occurs at $\overline{n}$ in all cases. With this input we can invert the truncated series (20) to get g_4 in terms of renormalized couplings:

$$g_4 = g_{4R} - g_{6R}\left(\frac{I_1}{2}\right) + \frac{g_{8R}}{2}\left(\frac{I_1}{2}\right)^2 - \frac{g_{10R}}{3!}\left(\frac{I_1}{2}\right)^3 + \cdots + \frac{g_{\overline{n}R}}{(\overline{n}/2-2)!}\left(\frac{-I_1}{2}\right)^{(\overline{n}/2-2)} \tag{21}$$

and in this case we find alternating signs. In addition, due to the topology of the divergent diagrams, the same argument can be repeated with equivalent conclusions for the couplings with odd index, $g_3,\ g_5, \ldots, g_{(\overline{n}-1)}$.

From the general relation in (20), we evince the result that couplings with even (odd) index n get divergent corrections only from other couplings with even (odd) index m, such that $n < m \leq \overline{n}$. Then, couplings with $n > \overline{n}$, that do not appear in the bare action (15), get only finite corrections from subleading diagrams that contain more than one vertex. Therefore, the theory is perturbatively renormalizable because all divergences are under control and can be discarded by the conventional insertion of counterterms in Eq. (15).

Depending on the value of $\overline{n}$, and therefore on the number of terms of the sum in Eq. (20), we get a larger or smaller correction to g_4. For instance, when $\overline{n} = 6$, g_4 gets only a logarithmic correction whereas for large $\overline{n}$, g_4 gets larger corrections that are proportional to higher powers of the logarithm, while the coupling $g_{\overline{n}-2}$ gets linear corrections in the logarithm and $g_{\overline{n}}$ does not have any divergent correction.

An interesting remark concerns the particular case in which all even couplings are equal ($g_4 = g_6 = g_8 = \cdots = g_{\overline{n}}$) and the right hand side of Eq. (20) becomes the truncated exponential series or, analogously, if $g_{4R} = g_{6R} = g_{8R} = \cdots = g_{\overline{n}R}$, Eq. (21) is the truncated exponential series with alternate signs. If we consider the limit $\overline{n} \to \infty$ under the assumption of equal couplings, we get from Eq. (20)

$$g_{4R} = g_4\, \mathrm{e}^{I_1/2}\ , \tag{22}$$

and the same result is obtained by starting from Eq. (21). In addition, it is evident that in the limit $\overline{n} \to \infty$ the relation between bare and renormalized coupling in Eq. (22) holds not only for the quartic coupling but for all couplings with even index and, as a consequence, if the bare couplings are all equal, then also the renormalized couplings are all equal (or viceversa). Clearly, all these results can be equivalently recovered for the set of couplings with odd index.

Equation (22) shows that, in order to keep g_{4R} finite when $\Lambda \to \infty$, g_4 must vanish in the same limit. Therefore, a peculiar result emerges for the exponential series where the couplings are all equal. Its extension to the more general case with different couplings g_n can be related to the possibility of constraining the given series of g_n with a suitably constructed exponential series which, for instance, is larger than the former, term by term (provided that $g_n > 0$ for all n). We can conclude that the more general series is summable, giving finite or vanishing g_n in the limit $\Lambda \to \infty$, and the associated model is UV safe or free.

Finally, the coefficients of the derivative terms, a_1, a_2, a_3, get corrections from diagrams that carry some external momentum dependence; this necessarily requires the presence of at least two vertices and consequently only UV finite corrections affect these three couplings. Therefore, the leading corrections come from the one loop diagram with two g_3 vertices and two internal lines, corresponding to the one loop integral $R_1(p)$ in Eq. (8), and from the two loop diagram with two g_4 vertices and three internal lines (sunset diagram) corresponding to the integral ($i\epsilon$ in the propagators is omitted)

$$R_2(p) = \int \frac{d^3k\, dk_0}{(2\pi)^4} \int \frac{d^3q\, dq_0}{(2\pi)^4}\, \frac{1}{k_0^2 - D(\vec{k})^2} \times \frac{1}{q_0^2 - D(\vec{q})^2}\, \frac{1}{(p_0+k_0+q_0)^2 - D(\vec{p}+\vec{k}+\vec{q})^2} \tag{23}$$

where, similarly to Eq. (9), we define

$$D(\vec{k}) = \sqrt{\widehat{a}_3\, \vec{k}^{\,6} + \widehat{a}_2\, \vec{k}^{\,4} + \widehat{a}_1\, \vec{k}^{\,2} + \widehat{g}_2}.$$

Then, explicitly, the leading corrections to a_1, a_2, a_3, are obtained from the coefficients of the expansion of these dia-

grams in powers of the external momentum $\vec{p}$ ($j = 1, 2, 3$)

$$\delta a_j = \frac{1}{(2j)!} \frac{\partial^{2j}}{(\partial|\vec{p}|)^{2j}} \left[\frac{i\,\widehat{g_3}^{\,2}}{2} R_1 - \frac{\widehat{g_4}^{\,2}}{6} R_2 \right] \Big|_{p=0} \tag{24}$$

The approximation in Eq. (24) represents the leading correction to the parameters a_j, both when $k \equiv |\vec{k}| >> M$ (and the propagators are dominated by the term $(a_3\, k^6/M^4)$), and when $k << M$ (and the dominant contribution to the propagator is now proportional to $a_1\, k^2$, while terms proportional to a_3 and a_2 are suppressed). In fact, further corrections to a_j involve more vertices $\widehat{g}_n$ with $n > 4$, and a higher number of loops. They are UV finite, according to the analysis of Sect. 2, and smaller in size than the leading corrections because of the numerical factor carried by each loop. Therefore, we do not include them in Eq. (24) where, in addition, we keep $\widehat{g}_3$ and $\widehat{g}_4$ constant, omitting higher order corrections related to the couplings. This implies that δa_j in (24) are independent of the specific value of $\overline{n}$ in Eq. (4).

An inspection of Eq. (24) in the UV region (i.e. when the momentum in the integrals R_1, R_2 is integrated from M to $\mu >> M$) shows the same power law behavior for the $O(\widehat{g_3}^{\,2})$ and $O(\widehat{g_4}^{\,2})$ corrections:

$$\delta a_j \propto \left(\frac{M}{\mu}\right)^{6+2j} . \tag{25}$$

Then, in this region a_1, a_2, a_3, get only negligible corrections and, for practical purposes, they maintain the value assigned in Eq. (17) (in particular $a_1 = a_3 = 1$).

In the IR region, i.e. when momentum is integrated from zero to $\mu << \sqrt{\widehat{g_2}} < M$, (provided $\widehat{g}_2 > 0$), all D, defined after Eq.(23), included in the propagators of R_1, R_2 in (24), are essentially proportional to $\sqrt{\widehat{g_2}}$, so that the contribution to δa_j is proportional to powers of $(\mu^2/\widehat{g_2})$, and therefore negligible.

The picture of the intermediate momentum region (with the integration variable ranging from $\mu \simeq \sqrt{\widehat{g_2}}$ to M), is less evident, since more than two scales are involved in the computation of R_1 and R_2, and a numerical analysis of Eq.(24) is in order. This analysis, discussed in Sect. 4, shows a negative correction $\delta a_3 < 0$ from the intermediate momentum region, with $|\delta a_3|$ proportional to the square couplings $\widehat{g}_3^2$ and $\widehat{g}_4^2$, as deducible from Eq. (24). It follows that there are particular conditions (a too small -or negative- $\widehat{g}_2$ and large couplings $\widehat{g}_3, \widehat{g}_4$) in which $\delta a_3 < -1$ and, after including these corrections in the factors D in Eq.(24), we end up with the square root of negative numbers. This singular behavior, appearing at IR scales close to $\sqrt{\widehat{g_2}}$, can be avoided by taking smaller $\widehat{g}_3$ and $\widehat{g}_4$, and/or larger $\widehat{g}_2$.

In addition, simple dimensional analysis of Eq.(24) shows that $|\delta a_2|$ and $|\delta a_1|$ are smaller than $|\delta a_3|$, respectively by the factors μ^2/M^2 and μ^4/M^4.

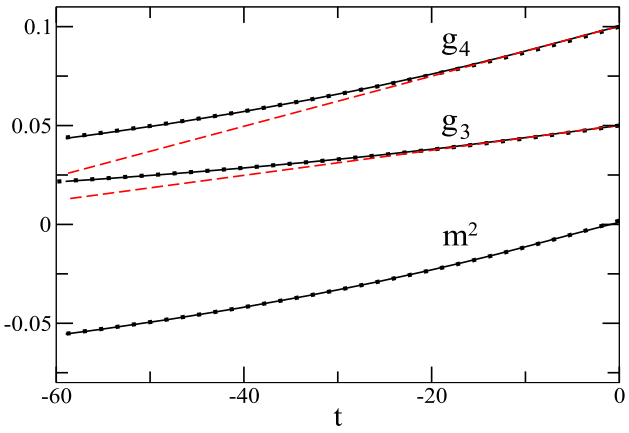

Fig. 1 UV flow of the couplings g_3, g_4, with boundaries fixed at $t = 0$, for two different values of $\overline{n}$, namely $\overline{n} = 22$, black solid lines, and $\overline{n} = 6$, red (online) dashed lines. At $t = 0$, for all g_n with n even and $4 \le n \le \overline{n}$, the boundary value 0.1 is used, while 0.05 is used for odd n. The flow of $m^2 = g_2$ is also displayed for $\overline{n} = 22$ with boundary value 10^{-3} for m^2 and the same boundaries as before for the other couplings. Dotted black lines correspond to the exponential approximation, as in Eq. (26), to the various curves

4 Flow of the couplings

By exploiting the dependence of the integrals on the renormalization scale, we easily transform Eq. (20) and the analogous relations for all the other couplings, into a set of differential flow equations for the scale dependent couplings $g_n(\mu)$, and study the evolution of the parameters with μ going toward the IR region at fixed boundaries at a large UV scale or, equivalently, explore the UV behavior by fixing the boundaries at a lower scale. To this purpose, we express all dimensionful quantities in terms of M and display the flow of the running $g_n(\mu)$ as a function of the logarithm of the scale μ: $t = \ln(M/\mu)$.

We start by investigating the UV region above M, where the effect of the modified propagator should be evident. We focus on some representative couplings, namely g_3 and g_4 plus the square mass term $m^2 = g_2$, as in this region a_1, a_2, a_3, that contribute to the propagator, remain practically constant. In Fig. 1 the UV behavior of the couplings g_3 and g_4 is studied by fixing the boundary conditions with all even couplings equal to 0.1 and all odd couplings equal to 0.05 at $t = 0$ (i.e. at $\mu = M$), for two different values of $\overline{n}$ in Eq. (4), namely $\overline{n} = 22$ (black solid curves) and $\overline{n} = 6$ (red dashed curves). Note that, according to the definitions given in Eq. (16), all values of the couplings are expressed in units of M.

The linear dependence of the red dashed curves is clearly evident. It is due to the choice $\overline{n} = 6$ which implies the contribution of a single one loop diagram to the flow of g_3 and g_4. The different slope of the two dashed curves is instead due to the different values of the vertices associated to the

one loop diagram respectively for g_3 and g_4. Conversely, the solid black lines are obtained for a very large value of $\overline{n}$, and we chose the same initial value of all even couplings and another initial value for all the odd couplings, with the aim of pointing out the exponential nature of the truncated series in Eq. (20). This trend is confirmed by the dotted black lines that reproduce the plot of the resummed exponential series shown in Eq. (22) which, in the present notation, becomes (for $j = 3, 4$)

$$g_j(t) = g_j(t = 0)\, e^{\frac{t}{8\pi^2}} \quad . \tag{26}$$

As already stated, at fixed $g_j(t = 0)$, the running couplings $g_j(t)$ vanish in the limit $t \to -\infty$.

Both dashed and solid lines are negatively divergent, the former linearly, as already noticed above, while the latter does actually diverge as a power of t due to the last term in the right hand side of Eq. (20) : $\sim (-g_{\overline{n}})\ (-t)^{(\overline{n}/2-2)}$ (according to our choice on the values of the couplings, $g_{\overline{n}}$ is the last non-vanishing coupling and does not get any correction).

Nevertheless, the divergent trend of the latter becomes evident only at extremely large negative values of t, not contained in Fig. 1, as an effect of the sum over the large number $\overline{n}$ of terms. On the contrary, Fig. 1 manifestly indicates that the exponentially vanishing expression in Eq. (26) provides an excellent approximation to the actual flow of our couplings up to $t = -60$ (i.e. $\mu/M \sim 10^{26}$) at least for the choice of the initial values of the couplings considered above.

If we select $\overline{n} = 24$ or $\overline{n} = 8$ in Fig. 1, instead of $\overline{n} = 22$ or $\overline{n} = 6$, then the dotted and dashed curves are modified because, according to Eq. (21), the couplings now tend to $+\infty$ as a power of $|t|$, when $t \to -\infty$, and a change of slope at some $t < 0$ with the generation of a minimum is observed. However, as discussed above, this change occurs at large $|t|$, the flow of g_4 and g_3 being dominated respectively by g_6 and g_5 at small $|t|$. In particular, for $\overline{n} = 24$ and the initial values used in Fig. 1, the trend of Eq. (26) is preserved for many orders of magnitude, up to $t = -60$, before the effects of g_{24} become apparent.

In Fig. 1 the square mass $m^2 = g_2$ is also plotted (solid line) for the case with $\overline{n} = 22$ and the boundary values of other couplings as declared above. The corresponding exponential curve is also reported (dotted line). Actually, the square mass in the UV region where the relevant scales are much larger than the mass itself, has the same of trend of the other couplings. Therefore, it is not surprising that its flow is totally similar to those already examined. The only difference is $m^2(t = 0) = 10^{-3}$, much smaller than the value of the other two couplings. In fact, we expect the renormalized mass of such a theory to be well below the Lorentz violating reference scale M, i.e. we expect $m^2 << 1$ at $t = 0$.

Let us now consider the momentum region around the scale M, corresponding to the transition from UV to IR

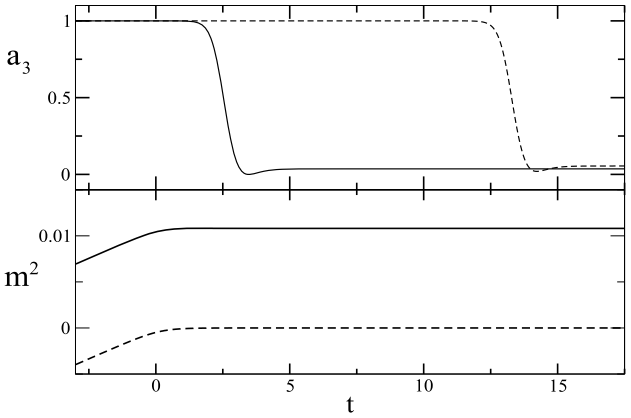

Fig. 2 Flow of the parameter a_3 (upper panel) and of the square mass $m^2 = g_2$ in the region around $t \sim 0$ and in the IR region with $t > 0$. Boundary values are taken at $t = -3$, with $m^2 = 0.007$ and $g_3 = g_4 = 0.1$ in one case (solid lines) and $m^2 \simeq -0.004$, $g_3 = 10^{-15}$, $g_4 = 0.1$ in the other case (dashed lines). As clarified in the text, diagrams containing vertices g_n, with $n > 4$, are neglected in this case and all plots do not depend on $\overline{n}$ in (4)

regime in which, due to the suppression of terms proportional to powers of k/M in the propagator, the onset of the well known standard scaling occurs. While no sensible change in the three coefficients a_1, a_2, a_3, is detectable in the UV region according to the explanation in Sect. 3, at momenta below M we expect a change in a_3 due to the finite corrections induced by the one and two loop diagrams, as shown in Eq.(24). However, for the sake of simplicity, in the following computation of the evolution of a_3, only the one loop diagram proportional to g_3^2 is included, while we neglect the two loop diagram proportional to g_4^2, subdominant with respect to the one loop diagram, because of the higher loop order.

The location of the change in a_3 is strictly related to the particular value of the square mass m^2. Therefore we report in the same figure both running parameters, a_3 and m^2, namely the former in the upper panel and the latter in the lower panel of Fig. 2, for two particular choices of the mass (solid and dashed lines in both panels). The boundary conditions are fixed at $t = -3$, and in the first case, that corresponds to the solid lines in Fig. 2, we take $g_3 = g_4 = 0.1$ and square mass $m^2 = 0.007$. The leading contribution to the flow of m^2, both above and below the scale M, comes from the one loop diagram proportional to g_4, whose effect is to increase the mass for growing t, although with different rates for $t < 0$ or $t > 0$ (in fact also the $O(g_3^2)$ one loop diagram is included but its contribution to the mass correction is practically negligible). Then, for large enough t, when the running scale becomes lower than the mass m, the flow of all couplings stops and this is clearly visible in all plots of Fig. 2.

According to all phenomenological indications, we expect the scale M to be various orders of magnitude larger than the IR mass of our model and this, despite the much softer behav-

ior of the parameters in the UV region, inevitably requires an accurate adjustment of the UV boundary value of m^2. So, unlike the first example in Fig. 2, where at large t we have $m^2 \simeq 10^{-2}$, in the second example corresponding to dashed curves, we tune the boundary value of $m^2(t = -3)$ at a negative value, and $g_3 = 10^{-15}$, to get in the IR region $m^2 \simeq 10^{-12}$. (Actually, the latter IR value of m^2 is chosen as a compromise between dealing with a very small but still numerically manageable number, and having a not too large physical mass, whose scale is set by M, which can be as large as, or larger than the Plank mass).

Figs.1, 2 show that our model produces a negatively growing m^2 when $t = \ln(M/\Lambda) \to -\infty$. Something similar occurs in the Lorentz invariant renormalizable $d = 4$ scalar theory but, while the latter provides a quadratically divergent $m^2 \propto -\Lambda^2$, in our model the quadratic trend occurs only below M (hardly visible in Fig. 2 because of the units chosen) while above M, it turns into the logarithmic trend shown in Fig 1.

In the upper panel of Fig. 2, the flow of a_3 is shown and a comparison of the solid and dashed lines indicates that the integration of the intermediate momentum region in Eq. (24) produces a rapid decrease of a_3, in correspondence of the the scale $t = \ln(M/m)$, where $m = m(t)$ is the corresponding value of the running mass, readable from the lower panel, i.e. $m \simeq \sqrt{0.01}$ for the solid line, and $m \simeq \sqrt{10^{-12}}$ for the dashed line. Above and below these crossover scales, both solid and dashed curves are essentially flat, indicating that $\delta a_3 \simeq 0$ in those regions, as suggested by the general analysis of Eq. (24) in Sect. 3.

However, as explained in Sect. 3, the drop of a_3 in Fig. 2 is proportional to the square coupling (g_3^2 in the present example) and if the running mass is too small, this can generate a negative argument of the square root in the factors D appearing in R_1 and R_2 in Eq. (24). To avoid this singular behavior, we choose a sufficiently large mass in the case of the solid line, while in the case of the dashed line where, as discussed above, we tuned the mass to the value $m \simeq 10^{-6}$, we must select the small value $g_3 \simeq 10^{-15}$.

As anticipated in the analysis of Eq.(24) in Sect. 3, the corrections δa_2 and δa_1 of the other two derivative couplings are suppressed with respect to δa_3. In fact, for the two examples discussed in Fig. 2, the numerical determination of the flow yields deviations from the boundary values $a_1 = 1, a_2 = a_2^B$ (as discussed before Eq. (17), a_2 is left unconstrained) that are small (especially δa_1) and of no practical relevance in this investigation and, therefore, negligible. Moreover, all numerical findings show small dependence on the specific value of $a_2^B \simeq O(1)$, so that, for the sake of simplicity, we take $a_2^B = 1$.

Finally, in Fig. 3 the crossover of the couplings g_4 (upper panel) and g_6 (lower panel) from one regime to the other is shown with the boundaries taken as in the two cases

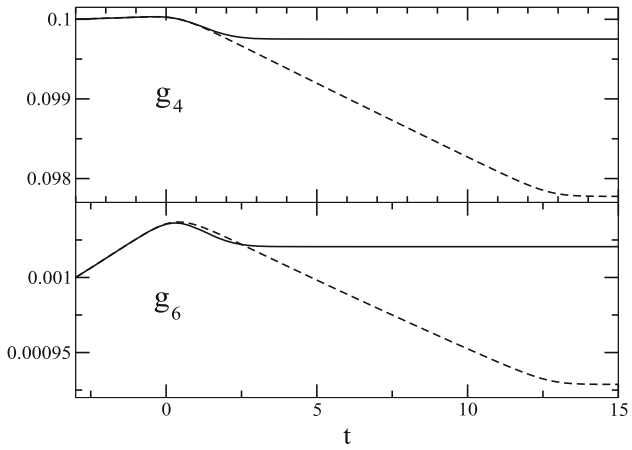

Fig. 3 Flow of g_4 (upper panel) and g_6 (lower panel) with the same boundary values (and the same coding) adopted in the two cases displayed in Fig. 2, with further boundary values: $g_6 = g_8 = 0.001$ at $t = -3$

already discussed in Fig. 2. So, solid lines correspond to large positive square mass at $t = -3$, while dashed lines to $m^2(t = -3) < 0$ and $g_3 \simeq 10^{-15}$. In both cases we fixed $g_4 = 0.1$ and $g_6 = g_8 = 0.001$ at $t = -3$. In addition, we do not include diagrams containing vertices g_n with $n > 8$ which, as discussed below, in this momentum region are finite and of higher order in the pertubative expansion, and therefore numerically negligible. This in turn implies that, similarly to δa_j in (24), the flow of g_4 and g_6 in this region is independent of the specific value of $\overline{n}$ in Eq. (4).

Both g_4 and g_6 show similar trends: increasing for $t < 0$ (due to the different scale in the two panels, the slope of g_4 is less evident although equal to that of g_6) and decreasing for $t > 0$ and finally flat at larger t, when the momentum scale becomes smaller than the mass m. The change of slope around $t = 0$ is a clear indication of the different influence of various diagrams in the two regions.

In fact, when $t < 0$, as repeatedly discussed, the relevant contribution comes from the single vertex, one loop diagram, which is $O(g_6)$ in the flow of the coupling g_4 and $O(g_8)$ in the flow of g_6 (note that we choose $g_6 = g_8$ in Fig. 3).

When $t > 0$, the term $\widehat{a}_1 k^2 = a_1 k^2$ is dominant with respect to $\widehat{a}_2 k^4 = a_2 k^4/M^2$ and to $\widehat{a}_3 k^6 = a_3 k^6/M^4$ in the propagators of the theory, and it is easy to realize by simple dimensional analysis that the one loop diagrams relevant when $t < 0$ and mentioned above, are now suppressed by the factor $g_6\, e^{-2t}$ in the flow of g_4, and by the factor $g_8\, e^{-2t}$ in the flow of g_6. The same dimensional analysis also shows that the p-loop diagrams resummed (because of the same order) in Eq.(20) in the flow of g_4 when $t < 0$, are suppressed by the factor $g_{4+2p}\, e^{-2pt}$ in the same flow when $t > 0$. Therefore, they are less and less important when n grows, and a resummation like the one in Eq.(20) is meaningless when $t > 0$.

On the contrary, when $t > 0$, according to standard perturbation theory, the dominant one loop diagrams have two vertices, as signaled by the the change of slope of the curves. Namely, they are the $O(g_4^2)$ diagram for the flow of g_4 and the $O(g_4\, g_6)$ diagram for g_6, which are those utilized in the computation of the flows in Fig. 3.

5 Comments and conclusions

The first conclusion that emerges from the above analysis is that the specific higher derivative scalar theory considered in this paper does not produce Lorentz violating effects in the low energy sector, large enough to be in contradiction with experimental observations. In fact, the action in Eq. (15) generates quantum corrections that are strongly suppressed at high momentum because of the modified propagator, and its anisotropy parameter z is chosen to be $z = 3$, the highest possible value at which the Lifshitz scaling protects the UV asymptotic behavior of the theory.

However, this is not sufficient to avoid dangerous corrections to a_1 that are responsible for the too large Lorentz violating effects, already observed in [37] for theories with $z = 2$. To avoid these effects, it is necessary to remove from the bare action all momentum dependent vertices, thus reducing precisely to the action in Eq. (15) where the vertices, which are all included in the potential V, do not contain any derivative of the field. In other words, we have to restrict our analysis in the parameter space around the fixed point solution (7), to the manifold in which all couplings associated to momentum dependent vertices are turned off. Clearly in the present form, this selection rule is not a consequence of some physical symmetry, but nevertheless, as explained in Sect. 2, it is self-consistent, in the sense that no UV divergent terms are generated, of the same kind of those not included in the bare action, and, moreover, it is sufficient to avoid those experimentally unacceptable effects.

In fact, the bare action (15) can be normalized by taking $a_1 = a_2 = a_3 = 1$, and then, the corrections found for a_3 are of the kind shown in the upper panel of Fig. 2, with the drop from $a_3 = 1$ to $a_3 \simeq 0$ occurring at a scale close to the mass m, while for a_1 and a_2 no significant correction is observed. Therefore, in the dispersion relation derived from Eq. (15) (which has the same form introduced in [49])

$$E^2 = \vec{k}^2 \left[a_1 + a_2 \left(\frac{k}{M}\right)^2 + a_3 \left(\frac{k}{M}\right)^4 \right] + m^2 \,, \qquad (27)$$

the suppression of the Lorentz violating terms in the relevant momentum region, $M >> k > m$, is essentially due to the factors $(k/M)^2$, and $(k/M)^4$, as no logarithmic correction affects a_1 and, in practice, in that region we still have $a_1 = a_2 = a_3 = 1$. If we accept the loose assumption that the same dispersion relation can be extended to more realistic theories and in particular to photons (but with $m = 0$), then, the experimental observations allow us to push the scale M around or above the lower limit $M > 10^{17}$ GeV [50]; however, conservatively, we have to retain this constraint just as a broad indication rather than a rigorous lower limit on M.

Concerning the renormalization of the theory with fixed $\overline{n}$ in Eq. (4), the divergent diagrams produced are all of the same kind, with logarithmic (and no quadratic) divergences. Therefore, the renormalization procedure is easy to handle and all divergences can be cured by means of the introduction of counterterms.

On the other hand, we can regard the action (15) as an effective theory with range of validity below some large UV momentum scale $\Lambda >> M$, and such that it reproduces the well known properties of a standard scalar theory in the IR momentum region below M. Then, the analysis of the RG flow indicates that, due to the presence of the Lifshitz point, this theory shows very small changes of the couplings in an extremely large range of the running scale μ (see Fig. 1). Not only all couplings are not divergent at some Landau pole below the scale Λ, but also they are, in practice, almost constant quantities.

However, since g_2, which is the square mass of the theory, shows, as the other couplings, only a small logarithmic change in the UV region well above M, but gets strong ($O(\mu^2)$) corrections below M (these are the large corrections which give rise to the naturalness problem), we must conclude that the smoothening of the flow above M does not influence the large changes in g_2 occurring at lower scales, so that the complication of fine tuning the UV value of the scalar mass is still present.

Finally, the case of very large $\overline{n}$ with almost equal values of the couplings needs to be emphasised. In fact, in Sect. 3 we noticed that the limiting theory where all couplings are equal, turns out to be asymptotically free with couplings that vanish when $\mu \to \infty$. (Incidentally, similarly to these findings, in [32–35] it is shown that the projectable Horava gravity model is renormalizable and asymptotically free both in 2+1 and 3+1 dimensions). It must be noticed that this limiting case shows a potential which is essentially equal to the one of the Liouville theory (and consequently the properties of the higher derivative four dimensional version of the Liouville theory certainly deserve further investigation), but at the same time, it can be used to bound more general theories.

In fact, if we treat Eq. (15) as an effective theory limited by an UV cutoff Λ, then the boundary condition at Λ, consisting of very similar (or at least of the same order of magnitude) small values for a huge number (or even an infinite) of adimensional couplings, could be accepted as a natural assumption. Then, a comparison with the Liouville potential should help in establishing constraints on the large momentum (but smaller than Λ) trend of the couplings of the effective theory

under investigation and, consequently, in testing whether the latter behaves effectively as an asymptotically free (or safe) theory.

Acknowledgements This work has been carried out within the INFN project FLAG.

Data Availability Statement This manuscript has no associated data or the data will not be deposited. [Authors' comment: All data and numerical results concerning the present study are all included in this article.]

Open Access This article is licensed under a Creative Commons Attribution 4.0 International License, which permits use, sharing, adaptation, distribution and reproduction in any medium or format, as long as you give appropriate credit to the original author(s) and the source, provide a link to the Creative Commons licence, and indicate if changes were made. The images or other third party material in this article are included in the article's Creative Commons licence, unless indicated otherwise in a credit line to the material. If material is not included in the article's Creative Commons licence and your intended use is not permitted by statutory regulation or exceeds the permitted use, you will need to obtain permission directly from the copyright holder. To view a copy of this licence, visit http://creativecommons.org/licenses/by/4.0/.
Funded by SCOAP[3].

References

1. W. Thirring, Regularization as a consequence of higher order equations. Phys. Rev. **77**, 570 (1950)
2. A. Pais, G.E. Uhlenbeck, On field theories with nonlocalized action. Phys. Rev. **79**, 145–165 (1950)
3. K.S. Stelle, Renormalization of higher derivative quantum gravity. Phys. Rev. D **16**, 953–969 (1977)
4. F.J. de Urries, J. Julve, Ostrogradski formalism for higher derivative scalar field theories. J. Phys. A **31**, 6949–6964 (1998). arXiv:hep-th/9802115
5. F.J. de Urries, J. Julve, E.J.S. Villasenor, Higher derivative boson field theories and constrained second order theories. J. Phys. A **34**, 8919–8940 (2001). arXiv:hep-th/0105301
6. S.W. Hawking, T. Hertog, Living with ghosts. Phys. Rev. D **65**, 103515 (2002). arXiv:hep-th/0107088
7. V.O. Rivelles, Triviality of higher derivative theories. Phys. Lett. B **577**, 137–142 (2003). arXiv:hep-th/0304073
8. A.V. Smilga, Benign versus malicious ghosts in higher-derivative theories. Nucl. Phys. B **706**, 598–614 (2005). arXiv:hep-th/0407231
9. S.I. Kruglov, Higher derivative scalar field theory in the first order formalism. Ann. Fond. Broglie **31**, 343–356 (2006). arXiv:hep-th/0606128
10. D. Anselmi, M. Halat, Renormalization of Lorentz violating theories. Phys. Rev. D **76**, 125011 (2007). arXiv:0707.2480
11. R. Hornreich, M. Luban, S. Shtrikman, Critical behavior at the onset of k-space instability on the λ line. Phys. Rev. Lett. **35**, 1678–1681 (1975)
12. R.M. Hornreich, The Lifshitz point: phase diagrams and critical behavior. J. Magn. Magn. Mater. **15**, 387–392 (1980)
13. W. Selke, The ANNNI model, Theoretical analysis and experimental application. Phys. Rep. **170**, 213–264 (1988)
14. H. Diehl, Critical behavior at M-axial Lifshitz points. Acta Phys. Slov. **52**, 271–283 (2002)
15. H. Diehl, M. Shpot, Critical, crossover, and correction to scaling exponents for isotropic Lifshitz points to order (8 - d)**2. J. Phys. A **35**, 6249–6260 (2002). arXiv:cond-mat/0204267
16. A. Bonanno, D. Zappala, Isotropic Lifshitz critical behavior from the functional renormalization group. Nucl. Phys. B **893**, 501–511 (2015). arXiv:1412.7046
17. D. Zappala, Isotropic Lifshitz point in the O(N) theory. Phys. Lett. B **773**, 213–218 (2017). arXiv:1703.00791
18. D. Zappala, Indications of isotropic Lifshitz points in four dimensions. Phys. Rev. D **98**(8), 085005 (2018). arXiv:1806.00043
19. D. Zappala, Isotropic Lifshitz scaling in four dimensions. Int. J. Geom. Meth. Mod. Phys. **17**(04), 2050053 (2020). arXiv:1912.03071
20. N. Defenu, A. Trombettoni, D. Zappala, Topological phase transitions in four dimensions. arXiv:2003.04909
21. R.P. Woodard, Avoiding dark energy with 1/r modifications of gravity. Lect. Notes Phys. **720**, 403–433 (2007). arXiv:astro-ph/0601672
22. S. Chadha, H.B. Nielsen, Lorentz invariance as a low-energy phenomenon. Nucl. Phys. B **217**, 125–144 (1983)
23. P. Horava, Quantum gravity at a Lifshitz point. Phys. Rev. D **79**, 084008 (2009). arXiv:0901.3775
24. R.-G. Cai, L.-M. Cao, N. Ohta, Thermodynamics of black holes in Horava–Lifshitz gravity. Phys. Lett. B **679**, 504–509 (2009). arXiv:0905.0751
25. R. Brandenberger, Matter bounce in Horava–Lifshitz cosmology. Phys. Rev. D **80**, 043516 (2009). arXiv:0904.2835
26. T. Takahashi, J. Soda, Chiral primordial gravitational waves from a Lifshitz point. Phys. Rev. Lett. **102**, 231301 (2009). arXiv:0904.0554
27. E. Kiritsis, G. Kofinas, Horava–Lifshitz cosmology. Nucl. Phys. B **821**, 467–480 (2009). arXiv:0904.1334
28. G. Calcagni, Cosmology of the Lifshitz universe. JHEP **09**, 112 (2009). arXiv:0904.0829
29. E.J. Son, W. Kim, Smooth cosmological phase transition in the Horava–Lifshitz gravity. JCAP **06**, 025 (2010). arXiv:1003.3055
30. M. Eune, W. Kim, Lifshitz scalar, brick wall method, and GUP in Horava–Lifshitz gravity. Phys. Rev. D **82**, 124048 (2010). arXiv:1007.1824
31. G. Cognola, R. Myrzakulov, L. Sebastiani, S. Vagnozzi, S. Zerbini, Covariant Horava-like and mimetic Horndeski gravity: cosmological solutions and perturbations. Class. Quantum Gravity **33**, 225014 (2016)
32. A.O. Barvinsky, D. Blas, M. Herrero-Valea, S.M. Sibiryakov, C.F. Steinwachs, Renormalization of Horava gravity. Phys. Rev. D **93**, 064022 (2016). arXiv:1512.02250
33. A.O. Barvinsky, D. Blas, M. Herrero-Valea, S.M. Sibiryakov, C.F. Steinwachs, Horava gravity is asymptotically free in 2+1 dimensions. Phys. Rev. Lett. **119**, 211301 (2017). arXiv:1706.06809
34. A.O. Barvinsky, D. Blas, M. Herrero-Valea, S.M. Sibiryakov, Towards the renormalization group flow of Horava gravity in 3+1 dimensions. Phys. Rev. D **100**, 026012 (2019). arXiv:1905.03798
35. A.O. Barvinsky, A.V. Kurov, S.M. Sibiryakov, Beta functions of (3+1)-dimensional projectable Horava gravity. Phys. Rev. D **105**, 044009 (2022). arXiv:2110.14688
36. P. Horava, Quantum criticality and Yang–Mills gauge theory. Phys. Lett. B **694**, 172–176 (2011). arXiv:0811.2217
37. R. Iengo, J.G. Russo, M. Serone, Renormalization group in Lifshitz-type theories. JHEP **11**, 020 (2009). arXiv:0906.3477
38. A. Dhar, G. Mandal, S.R. Wadia, Asymptotically free four-fermi theory in 4 dimensions at the z = 3 Lifshitz-like fixed point. Phys. Rev. D **80**, 105018 (2009). arXiv:0905.2928
39. K. Kikuchi, Restoration of Lorentz symmetry for Lifshitz type scalar theory. Prog. Theor. Phys. **127**, 409–431 (2012). arXiv:1111.6075

40. M. Eune, W. Kim, E.J. Son, Effective potentials in the Lifshitz scalar field theory. Phys. Lett. B **703**, 100–105 (2011). arXiv:1105.5194
41. J. Alexandre, Lifshitz-type quantum field theories in particle physics. Int. J. Mod. Phys. A **26**, 4523–4541 (2011). arXiv:1109.5629
42. W. Chao, Horava—Lifshitz type quantum field theory and hierarchy problem. Commun. Theor. Phys. **65**(6), 743–746 (2016). arXiv:0911.4709
43. A.R. Solomon , M. Trodden, Higher-derivative operators and effective field theory for general scalar-tensor theories. JCAP **02**, 031 (2018). arXiv:1709.09695
44. C. Farias, M. Gomes, J. Nascimento, A. Petrov, A. da Silva, On the effective potential for Horava–Lifshitz-like theories. Phys. Rev. D **85**, 127701 (2012). arXiv:1112.2081
45. A. Bonanno, M. Park, L. Rachwał, D. Zappalà, On the regularization of Lifshitz-type field theories. Eur. Phys. J. C **80**(11), 1081 (2020). arXiv:2010.05966
46. R.B. Paris , M.A. Shpot, A Feynman integral in Lifshitz-point and Lorentz-violating theories in $R^D \oplus R^m$. Math. Methods Appl. Sci. **41**(5), 2220–2246 (2018). arXiv:1707.03018
47. J. Collins, A. Perez, D. Sudarsky, L. Urrutia, H. Vucetich, Lorentz invariance and quantum gravity: an additional fine-tuning problem? Phys. Rev. Lett. **93**, 191301 (2004). arXiv:gr-qc/0403053
48. J. Collins, A. Perez, D. Sudarsky, Lorentz invariance violation and its role in quantum gravity phenomenology. arXiv:hep-th/0603002
49. S.R. Coleman, S.L. Glashow, High-energy tests of Lorentz invariance. Phys. Rev. D **59**, 116008 (1999). arXiv:hep-ph/9812418
50. J. Ellis, R. Konoplich, N.E. Mavromatos, L. Nguyen, A.S. Sakharov, E.K. Sarkisyan-Grinbaum, Robust constraint on Lorentz violation using fermi-LAT gamma-ray burst data. Phys. Rev. D **99**(8), 083009 (2019). arXiv:1807.00189